J. Fluid Mech. (1999), *vol.* 394, *pp.* 339–354. Printed in the United Kingdom

Experimental study of rivulet formation on an inclined plate by fluorescent imaging

By M. F. G. JOHNSON[1], R. A. SCHLUTER[2], M. J. MIKSIS[3] AND S. G. BANKOFF[4]

[1] Department of Mechanical Engineering
[2] Department of Physics and Astronomy
[3] Department of Engineering Science and Applied Mathematics
[4] Department of Chemical Engineering

Northwestern University, Evanston, IL 60208, USA

(Received 16 October 1997 and in revised form 5 April 1999)

The instability of a two-dimensional moving contact line is studied for a thin liquid film flowing down an inclined plane, leading to the formation of rivulets. A fluorescent imaging method was developed to facilitate accurate measurement of the spacing between rivulets, tip velocity, three-dimensional shape and dynamic contact line. A fluid circulation system produced steady films at constant volumetric flux, in contrast to time-varying films at constant total volume, as in previous measurements. Comparisons are made with the existing data for constant-volume films, and with theoretical predictions for the wavelength of the rivulets formed at constant inlet flow rate. Data were also obtained for rivulet shapes, tip speeds and contact angles as functions of the angle of inclination of the plate and liquid Reynolds number.

1. Introduction

The need for better understanding of the flow characteristics of a thin film of fluid arises in the coating of dry surfaces, such as in the manufacture of photographic film or computer chips, where uniformity and completeness of wetting are paramount in importance. A fundamental geometry is the simple wetting of a dry inclined plate by a thin, uniform liquid film draining under gravity. This paper deals with an experimental investigation of this problem, using water–glycerin mixtures containing a small amount of dissolved fluorescein flowing on a glass plate. In contrast with previous work on this problem, the fluid flux in the unbroken film is constant. When illuminated by ultraviolet light, the local intensity of fluorescent light emitted is nearly proportional to the local film thickness. A similar method has been described by Liu, Paul & Gollub (1993) for the study of pattern development of surface waves on a liquid film flowing down an inclined plate, but a number of refinements (Johnson, Schluter & Bankoff 1997) were required to adapt the method to the study of moving contact lines and dynamic contact angles. This involved the measurement over a fairly large region of wavelength, film thickness and dynamic contact angle during the onset of fingering and during the development and propagation of rivulets. The experimental method described in this paper allowed the measurement within one degree of the macroscopic dynamic angle of a moving fluid front, taken from a tangent line drawn at the face of the rivulet. Experimental values could be recorded at any point in time and at any location within the approximately 1 m^2 flow field. In

addition, data were obtained for rivulet formation along a plate inclined at angles of 6° to 25° to the horizontal, and also on a vertical plate.

2. Background

In the presence of body forces, such as gravity or centrifugal forces, the leading edge of a thin coating flow is unstable. In the case of an inclined plate, an initially straight leading edge, i.e. the contact line, is unstable to lateral perturbations, which can develop into well-defined finger-like structures or rivulets. As first demonstrated by Huppert (1982), the shape of the rivulets may be a triangular sawtooth configuration, where the roots move more slowly than the tips, or may be an array of straight-sided, constant-width finger-type rivulets, whose roots may appear to be stationary. The stationary roots are generally undesirable since they lead to incomplete coverage of the plate for all time. Silvi & Dussan V. (1985) show that a large contact angle promotes the formation of finger-type rivulets. Here we will show a transition from sawtooth to finger rivulets as the angle of inclination of the plate is increased. In addition, in our experiments the velocity of the roots of the finger rivulets is less than that of the sawtooth rivulets, but the roots never become stationary, in contrast to the observations of Huppert (1982), Silvi & Dussan V. (1985) and de Bruyn (1992) in fixed-volume experiments. Related fixed-volume experiments were performed by Goodwin (1991) with water–glycerin mixtures on an inclined plate, Spaid & Homsy (1996) with viscoelastic liquids, and Melo, Joanny & Fauve (1989) and Fraysse & Homsy (1993) for spin coating. Finally, we note that there have been numerous theoretical investigations of the problem, e.g. Troian *et al.* (1989), Spaid & Homsy (1996), Lopez, Bankoff & Miksis (1996), Lopez, Miksis & Bankoff (1997), Bertozzi & Brenner (1997), but the dynamics of the coating flow are still not well understood. For example, the conditions under which we can expect fingers or sawtooth rivulets, and the structure and dynamics of the leading edge of the rivulets, are unknown. Some of these issues will be addressed here.

3. Experimental facility

The experimental facility for the constant flow rate studies of a draining film is diagrammed in figure 1. Two banks of ultraviolet bulbs flank the Sony XC-75 CCD camera, to which one of two lenses, a Fujinon TV zoom lens (16–160 mm) or a higher resolution Bolex-Lyar (25 mm) is attached. The Fujinon lens permits a viewing range from 2×3 cm to 50×79 cm. The glass surface over which the thin film flows is mounted on a $0.77\,\mathrm{m} \times 0.95$ mm aluminium plate, painted black to eliminate unwanted reflections. The thin liquid film is a saturated solution of fluorescein in a mixture of glycerin and water. The film becomes fluorescent when exposed to ultraviolet light with an intensity proportional to the local film thickness. The addition of fluorescein was shown to affect fluid properties (viscosity, surface tension and density) by less than the error of measurement of these properties ($<2\%$) by direct comparison with mixtures without the dye. Most of the data presented herein were for a glycerin–water mixture with a weight percentage of 33%, labelled Fluid A, or 80%, labelled Fluid B. Two other fluid mixtures were used for only the wavelength data (labelled C and D). We will give a brief overview of the fluorescent imaging method below. Details of the method can be found in Johnson *et al.* (1997).

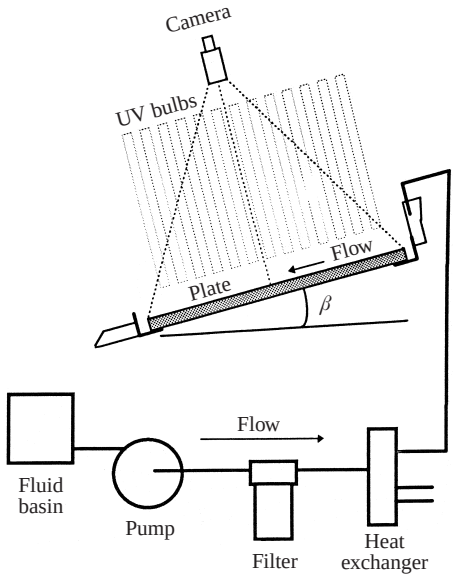

FIGURE 1. Side view of the experimental facility showing fluid flow and optical systems.

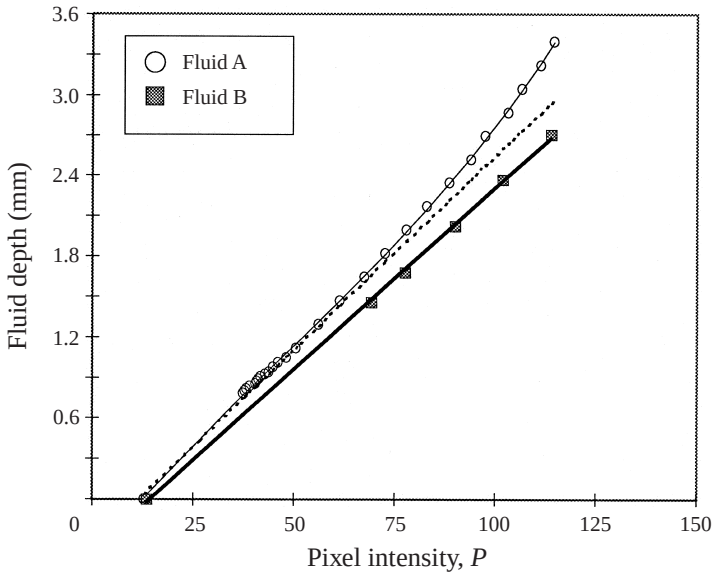

FIGURE 2. Calibration curve for converting pixel intensity values to actual fluid depth values. The dotted line represents a straight-line extrapolation to show the deviation from a linear fit due to absorption effects.

3.1. *Fluorescent imaging method*

In order to measure fluid depths an imaging software (Image-Pro Plus v. 1.3) was used that records the fluorescence level emitted by the fluid. The intensity and location of each pixel were recorded, and converted into a local film thickness from a calibration curve, as in figure 2. The curve is determined for a fluid by recording the fluorescent intensity for several known volumes of fluid contained within a shallow cylindrical dish. A zero fluid depth value did not correspond to a fluorescent intensity of zero,

but had a value dependent on the aperture setting of the camera. This method has a variation of approximately ± 0.02 mm, due mainly to variations of the recorded fluorescent values using the imaging software. Typically about ten values for the intensity were used to determine each point on a fluid depth calibration curve. Johnson *et al.* (1997) note that depending on the absorption depth property of the fluid (both the incoming UV and outgoing fluorescence), the calibration curve in figure 2 can be slightly nonlinear. This is true for Fluid A, where the calibration curve begins to deviate from linear at about a depth of 1 mm. Fluid B also exhibits the same nonlinear effect, but at depths of over 5 mm.

The method as described would accurately measure fluid depth values where variations in the fluid depth are relatively small, including small surface waves on a continuous film. Corrections are required in the neighbourhood of the contact line for non-wetting fluids (Johnson *et al.* 1997) and arise from additional UV light capture, approximately proportional to the slope of the fluid surface, and also the effective optical resolution of the system. The measurement of fluid boundary shape and fluid depth behind a contact line does not depend critically on optical resolution. However, detail at the contact line vertex is limited by three effects: (i) optical resolution of the lens, (ii) light scattering (lack of contrast) in the lens, and (iii) digital camera pixel size. Comparison of fluid depth shapes measured directly using a shadow tracing method and the fluorescent imaging method show that the light scattering effect is negligible for cases where the contact angle is less than 20°. Pixel numbers were converted to lengths by recording an image of known length and counting the number of pixel points corresponding to this length.

3.2. *Developing a two-dimensional fluid front*

Data are presented here for varying flow rates and inclination angles to the horizontal from 6° to 90°. Data for plate angles less than 30° were recorded using the apparatus shown in figure 1. A separate experimental facility was used for an angle of inclination of 90°. Initially liquid was allowed to flow from a reservoir behind the top of the plate onto the surface of the 768 mm × 946 mm plate, as shown in figure 1. This method worked reasonably well, except for angles of inclination less than 10°, where edge irregularities prevented the formation of a uniform front. Because of the problems associated with the low angles of inclination and with the need to clean the surface after each run, an alternative method for forming a flat fluid front was developed. This method used a 457 mm long rubber wedge (window washer 'squeegee') to remove a section of fluid from a continuous film (figure 3). The squeegee method resulted in a uniform initial front for all plate angles. However, the squeegee leaves behind a very thin film of liquid, measured to be approximately 10 microns. At larger angles of inclination (>10°) the overflow reservoir method produced rivulets within experimental error of the same wavelength as the rivulets formed using the squeegee method. Thus the existence of a dry plate or the presence of a microscopic film appeared, at least for the larger angles of inclination, to have a negligible effect on the fluid flow instability forming rivulets.

There was concern that the squeegee might interfere with the initial formation of the two-dimensional front from which the rivulets formed. Specifically, there was a question whether the squeegee could cause a build-up of fluid at the fluid front, forming an artificial hump, instead of the natural hump that is an essential part of the instability leading to the formation of rivulets. Figure 4 shows a time series of fluid depth cross-section profiles taken in the direction of flow (x-direction). Time zero corresponds to the instant right after the application of the squeegee. One sees that

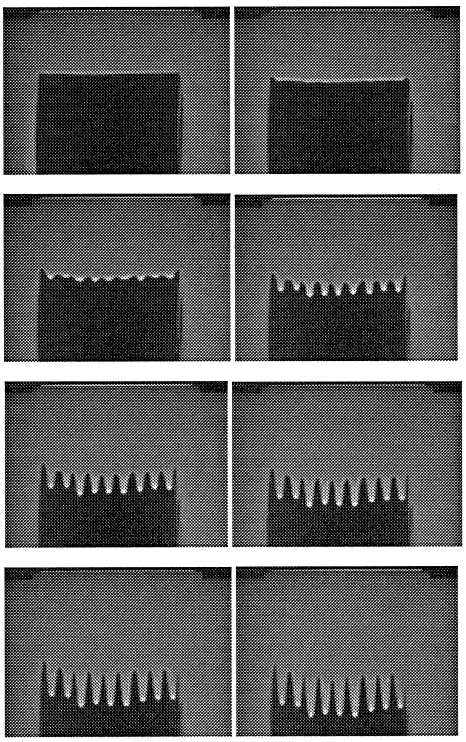

FIGURE 3. Flow images taken at 1 s intervals showing the evolution of a two-dimensional fluid front forming rivulets for Fluid B.

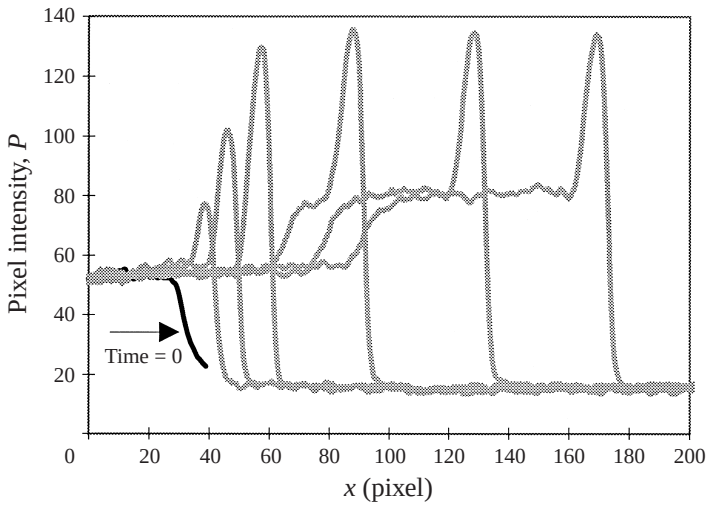

FIGURE 4. Time evolution for the formation of a two-dimensional fluid front formed using the squeegee method. 1 pixel = 0.88 mm.

the squeegee actually cuts the thin film cleanly, forming a two-dimensional fluid front without a hump, as shown by the fluid depth profile taken at time zero. Fluid depth values for this line at points for $x > 40$ pixels were unavailable due to the squeegee being in the field of view of the flow image. As time increases a rivulet forms from the flat two-dimensional front and then continues flowing down the plate.

	Density ($\pm 5\,\mathrm{kg\,m^{-3}}$)	Kinematic viscosity ($\pm 1 \times 10^{-6}\,\mathrm{m^2\,s^{-1}}$)	Surface tension ($\pm 0.002\,\mathrm{kg\,s^{-2}}$)	weight %, glycerin (%)
Fluid A	1075	2.9×10^{-5}	0.069	33
Fluid B	1210	6.9×10^{-5}	0.066	80
Fluid C	1200	6.3×10^{-5}	0.067	77
Fluid D	1120	6.0×10^{-5}	0.070	48

TABLE 1. Fluid properties of experimental fluids at 21 °C.

β (deg.)	Re (± 0.06)	Ca	d_{0m} (mm)	d_0 (mm)
23.3	0.6	0.01	0.80	0.74
23.3	2.4	0.03	1.24	1.17
23.3	4.6	0.04	1.50	1.46
14.5	0.6	0.01	0.92	0.86
14.5	2.4	0.02	1.45	1.37
14.5	4.6	0.04	1.79	1.70
6.0	0.6	0.01	1.26	1.15
6.0	2.4	0.02	1.92	1.83
6.0	4.6	0.03	2.34	2.27

TABLE 2. Measured fluid depths (d_{0m}) and calculated depth (d_0) for a continuous film for fluid A.

4. Experimental results

Experimental results are reported as functions of angle of inclination of the plate (β), the Reynolds number (Re) representing the volumetric flow rate per unit width (Q) and the capillary number (Ca). Early inspection of the data showed that changes in these parameters had a significant effect on the shape and spacing of the rivulets. In order to see if inertia had any effect on the flow, data were obtained for Re in the range of 0.3–5.0. The capillary number is defined as

$$Ca = Q\rho v/d_0\sigma, \tag{1}$$

where Q is the volumetric flow rate per unit width, and the density (ρ), surface tension (σ) and kinematic viscosity (v) are given in table 1. The Reynolds number is defined as $Re = Q/v$. The value for the theoretical fluid depth (d_0) is defined below in equation (2). Since both the capillary number and the Reynolds number are proportional to the flow rate Q, either would be a natural parameter to use in our study. Because of its simple relationship to the flow rate, the Reynolds number is preferable. However it may not be the critical parameter. For thin films as studied here, lubrication theory is valid and it has been shown in several theoretical investigations (e.g. Huppert 1982) that the capillary number is the critical parameter in these theories. Here we will report both the Reynolds and capillary numbers.

Table 2 shows the bulk fluid depth (d_{0m}), measured for a continuous film as a function of the angle of inclination, the Reynolds number, Re and the capillary number, Ca. Also given are the values of the theoretical fluid depth (d_0):

$$d_0 = [3Qv/g\sin\beta]^{1/3} \tag{2}$$

for thin films flowing down an inclined plane at constant flux. In equation (2), g is the gravitational constant. Each measured value in table 2 represents the average of

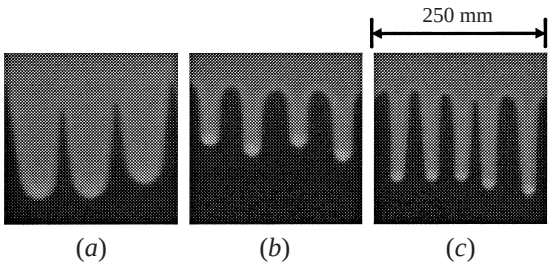

FIGURE 5. Rivulet patterns formed by a water/glycerin mixture for (*a*) $\beta = 6.2°$, (*b*) 15.8° and (*c*) 23.8° and *Re* approximately equal to 1, for Fluid A.

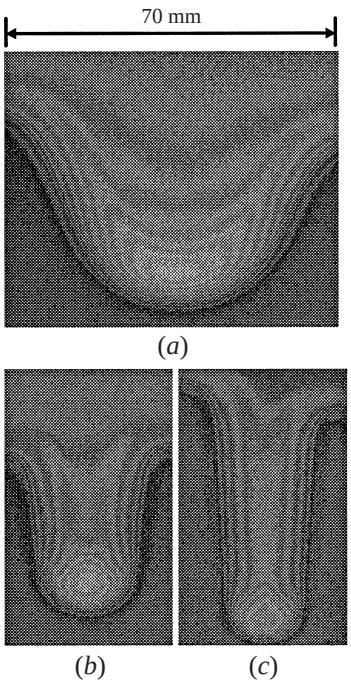

FIGURE 6. Contour maps of rivulet formed by Fluid A for varying angles of inclination: (*a*) $\beta = 6.2°$, (*b*) 15.8°, (*c*) 23.8°.

about three to five test runs with an average variation of about ± 0.04 mm for each value of d_{0m} and ± 0.06 for each value of *Re*.

Note that the measured values are consistently larger than the calculated values by an average of 5%. This difference is attributed to small surface waves which dissipate energy, resulting in a slightly thicker film than calculated from equation (2). Hence we find reasonable comparison between theory and experiment for this easily obtained quantity.

4.1. *Fluid depth profiles*

Using the values of the parameters listed above, measurements were made of the moving interface and the resulting rivulets. Examples are given in figures 5 and 6, where the images of the rivulets were recorded once the rivulets had travelled the same distance down the incline. Note that the rivulets are not of the same length, since the roots move at a different speed for each flow condition.

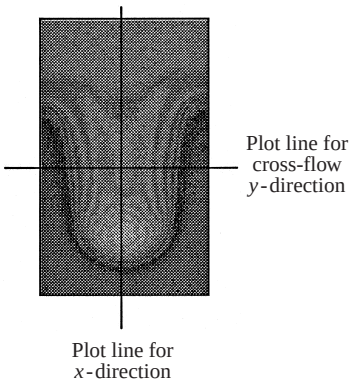

FIGURE 7. Plot lines used for depth profiles of rivulets in the cross-flow and flow directions.

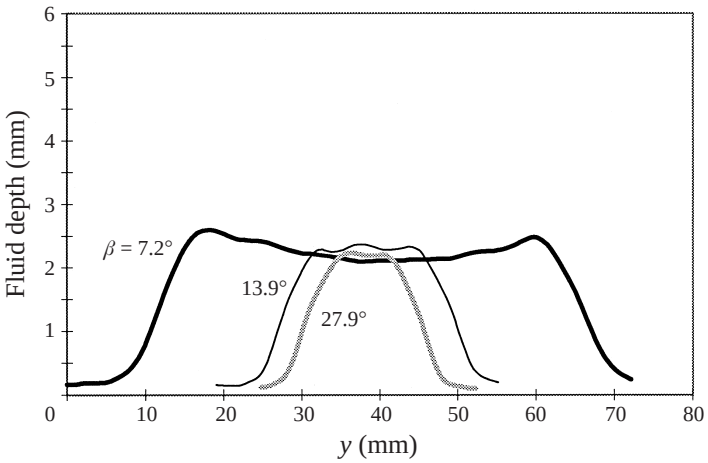

FIGURE 8. Cross-sectional depth profile of rivulet formed for $Re = 0.13$ with Fluid B. Three profiles are shown for $\beta = 7.2°$, 13.9° and 27.9° with corresponding $Ca = 0.010$, 0.012 and 0.015.

Figure 5 shows some features of the rivulets formed by using the squeegee method for $Re \approx 1$. The width of the rivulets is greater at the smaller angles of inclination, while the spacing between them decreases as the angle of inclination is increased. The rivulets form a sawtooth pattern at a plate angle of inclination of 6.2°, similar to that observed by Huppert (1982), Silvi & Dussan V. (1985) and de Bruyn (1992), with the entire plate being coated as the roots move down the incline.

Data for fluid depth obtained using the fluorescent imaging method are shown in figure 6. The figure shows contour maps of rivulets formed for a flow with $Re = 1$ and at angles of inclination, $\beta = 6.2°$, 15.8° and 23.8°. The images have been enhanced using a banded grey scale to show the contours representing the fluid depth of the rivulets. The contour maps show that a hump forms at the leading edge of the three-dimensional front, which extends along the sides of the rivulets. This rivulet structure is similar to the rivulets formed by spinning drops (Melo *et al.* 1989) and to that for a front driven vertically upwards by thermal gradients (Cazabat *et al.* 1990). Some axial and cross-sectional profiles are plotted along the lines shown in figure 7. The fluid depth profiles presented here are for Fluid B only, but similar results were obtained for Fluid A. Figure 8 is a plot of the fluid depth profile taken in the lateral (y) direction at the midpoint between the tip and root of the rivulets. One

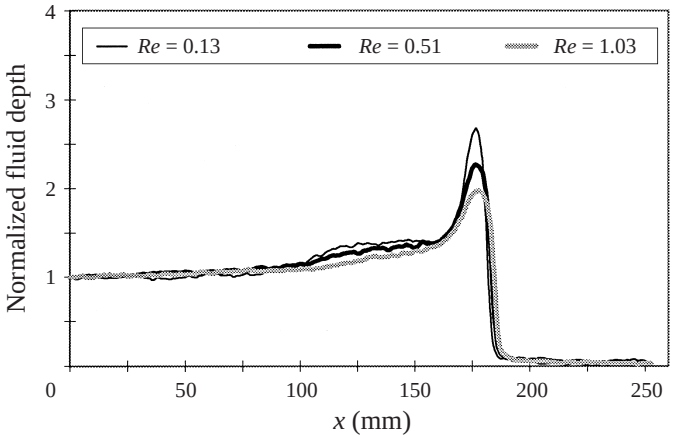

FIGURE 9. Normalized Fluid B depth as a function of distance in the direction of flow for $\beta = 13.9°$, and $Re = 0.13$, 0.51 and 1.03 with corresponding $Ca = 0.012$, 0.031, and 0.049.

sees a plateau or valley between the ridges along the sides of the rivulets for $\beta = 7.2°$ and 13.9°. This is a feature that has not been previously reported in the literature. Theoretical models to date have only calculated the shape of a two-dimensional flow with a contact line or precursor film along the direction of flow (x-direction). Recent numerical calculations by Moyle, Chen & Homsy (1999) show a similar shape for sawtooth and finger rivulets, but without the ridge along the sides. The cross-sections of the rivulets become more rounded as β increases, because the ridges have merged together, eliminating the valley. The rounding of the lateral shape of the rivulets is due to the decreasing effect of gravity on the interfacial shape as the angle of the plate is increased. The rivulets form an almost perfect semi-circular shape on the vertical wall where the normal component of gravity is nearly zero. The sides of the flatter rivulets were also observed to have a larger velocity in the lateral direction than the finger-type rivulets at higher plate angles. Data for Fluid B also showed a linear increase in this velocity as the Reynolds number was increased. This was accomplished by an increase in the dynamic contact angle at the sides of the rivulets.

Two-dimensional models by Lopez *et al.* (1996) Goodwin & Homsy (1991), Spaid & Homsy (1996), Hocking (1990) and Troian *et al.* (1989) show that the shape of the fluid front consists of a hump at the leading edge, which flattens to a uniform fluid depth at a point far upstream. Figure 9 represents a sample of rivulet fluid depth profiles for $\beta = 13.9°$ and varying Reynolds number and the associated capillary number. Measurements are taken along the centreline of the rivulet. The ordinate is the fluid depth divided by the bulk film depth (d_{0m}) as measured upstream from the rivulet front. This figure, as well as others, appears to show a small foot-like structure located at the region in front of the fluid hump extending to the plate surface. The structure has been shown by Johnson (1997) to be an optical effect that exists with this type of imaging system. Hence any structure that may exist in the region is undetectable using this imaging system. For example, in order for a precursor film to exist, Johnson *et al.* (1997) showed that the depth must be less than 0.05 mm, and hence invisible to the naked eye. This depth is the point where the fluid depth measured using the imaging system began significantly to differ from the known depth, and was determined by comparing the depth profile of a drop using a travelling microscope and a profile using the imaging system.

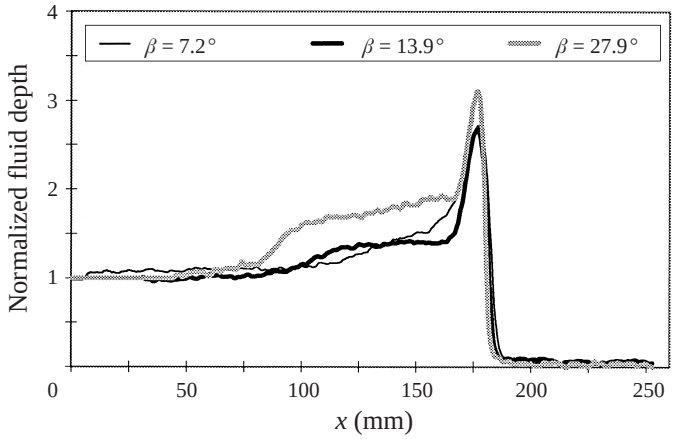

FIGURE 10. Normalized Fluid B depth as a function of distance in the direction of flow for $Re = 0.13$ and plate angle β.

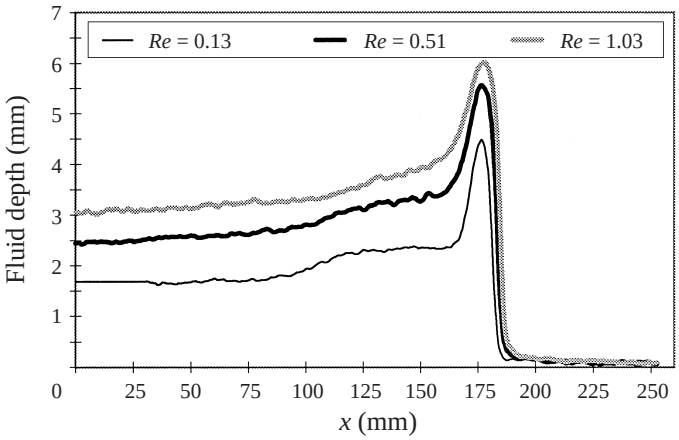

FIGURE 11. Plot of Fluid B depth as a function of distance in the direction of flow for $\beta = 13.9°$ and various Reynolds number.

One characteristic of the flow field is that the fluid depth along the centreline of the rivulet is relatively constant behind the hump at its head up to a point on the x-axis that corresponds to the location of its root. After this point the depth of the film decreases, as expected by conservation of mass. Figure 9 shows that the normalized hump height increases with decreasing Reynolds number and capillary number. This was also observed for other angles of inclination. Figure 10 shows the normalized fluid height for different values of β. The dimensionless hump height for the highest angle was more than for the lower plate angles, with the heights being virtually the same for $\beta = 7.2°$ and 13.9°. The same trend was also observed for fluid depth profiles with a range of $Re = 0.6$ to 4.6 for Fluid A. The same data plotted in figures 11 and 12 show, as expected, that the dimensional fluid depth (h) at all points along the axis of the rivulet decreases with decreasing Re and Ca. Differences in the hump height and shape are now evident. The maximum hump height of about 6.2 mm corresponds to the maximum Reynolds number of 1.03. The hump height decreases along with the rivulet depth as the value of Re is decreased, with the minimum height of 4.6 mm

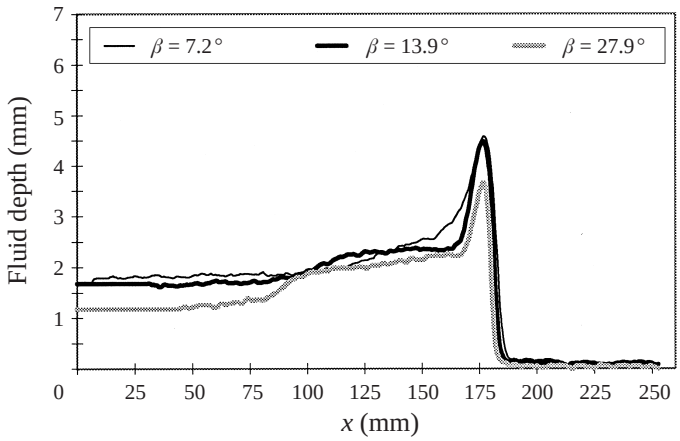

FIGURE 12. Plot of Fluid B depth as a function of distance in the direction of flow for $Re = 0.13$, $\beta = 7.2°$, 13.9° and 27.9° with corresponding $Ca = 0.010$, 0.012 and 0.015.

at $Re = 0.13$. Figure 12 gives data for constant Re and varying β, and shows a maximum hump height of 4.6 mm for $\beta = 7.2°$ and 13.9°, which decreases to 3.6 mm for $\beta = 27.9°$.

The figures for the rivulet fluid depth show that the back side of the hump has a smaller slope as β decreases. This leads to a related question of whether a critical angle exists below which the hump disappears for a two-dimensional front. Bertozzi & Brenner (1997) describe such a critical angle, below which the hump does not exist, and the two-dimensional fluid front becomes linearly stable. They further propose that for cases below the critical angle where no hump is present, fingering can still occur, due to nonlinear growth at the front caused by small perturbations there, related to the surface roughness to the plate. Their analysis assumed similar flow conditions to those of Huppert (1982), and found that the critical angle is within the experimental range of Huppert, leading to a critical angle slightly greater than 5°. This critical value is slightly smaller than the smallest value of β investigated above. Therefore, another front was produced using the squeegee method for $\beta = 1.8°$, which is well below their critical angle value. Data for this angle showed that the leading edge became unstable and a pronounced hump still existed at the front of the fluid. This result suggests that the linear instability mechanism for the formation of fingering associated with the presence of a hump is still dominant. We did observe that the hump was less pronounced or flatter as β decreases, but also the wavelength increases suggesting that the finite width of the plate may affect our results for these very low angles ($\beta = 1.8°$).

Another characteristic of the hump that can be measured using the fluorescent imaging system is the length (X_{hump}) along the x-direction from the front of the rivulet to the point corresponding to the hump fluid depth, h_{max}. The front or the tip of the rivulet is the point along the front just above the inflection point of the optically created foot, as discussed by Johnson (1997). The data show that X_{hump} increases by nearly 25% for all plate angles as Ca (and Re) increases for Fluid B. This appears to agree with the predictions for a steady two-dimensional coating flow model using lubrication theory (Spaid & Homsy 1996 and Lopez *et al.* 1996). The results also show that X_{hump} decreases as β increases which is again consistent with the lubrication result. Theoretical modelling of this three-dimensional rivulet is necessary before any

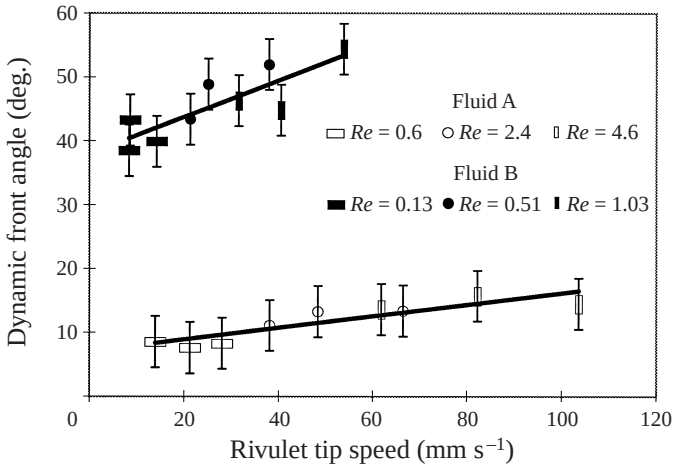

FIGURE 13. Data showing approximate linear relation between the speed and dynamic front angle at the tip of a rivulet.

additional comparisons between experiments and theory can be made. We note that Goodwin & Homsy (1991) plot X_{max}, a non-dimensional X_{hump}, on a log-log plot as a function of capillary number. They state that slopes of the resulting curves show whether a lubrication approximation is appropriate for the given experimental condition. In order for lubrication theory to apply, X_{max} must scale like $Ca^{-1/3}$. The exponent for X_{hump} as a function of Ca was determined by dividing X_{hump} by d_0 and fitting the data on a log-log plot. The resulting curve had a slope of 0.3, which suggests that the lubrication approximation would apply to the data for Fluid B. Some of the data, but not all, presented by Goodwin & Homsy (1991) had similar results. A larger value for the slope, giving a larger exponent on Ca, was found for conditions with contact angles above 50°.

With the ability to measure fluid depth, the rivulet front angle, which can be identified with the dynamic contact angle θ, can be measured at any point in the flow field at any time. The value for the front angle of the rivulets is measured at the intersection of the rivulet centreline and the contact line, and is obtained from the slope of the tangent fitted to the fluid depth values recorded at the front of the rivulet. The slope was determined at fluid depths greater than 0.05 mm, which is above the 'foot' seen in the fluid depth profiles. Johnson *et al.* (1997) showed this 'foot' to be an optical effect due to light scattering, geometric resolution of the camera lens and the resolution of the video system. The error associated with the measurement of the contact angle using this fluorescent method accounts for a variation of slightly greater than 1° due to the precision error for the measurement of the fluid depth. However, we did observe a variation of about 4° for the face angle of individual rivulets within the same flow field. The data for the dynamic contact angle are plotted in figure 13 as a function of the speed of the rivulet tips, U, for the different flow conditions. Results for Fluid A and B are presented.

We see that the relationship between θ and U is approximately linear. In particular it is found that $\theta = 0.29(U) + 38$ for Fluid A and $\theta = 0.09(U) + 7$ for Fluid B. The data were also fitted to some nonlinear forms, but the quality of fit was not better than for the linear form. We should note that several different relationships between the dynamic contact angle and the slip velocity have been proposed in the literature (Blake 1993), but for the data presented here, a linear fit seems the best. This may

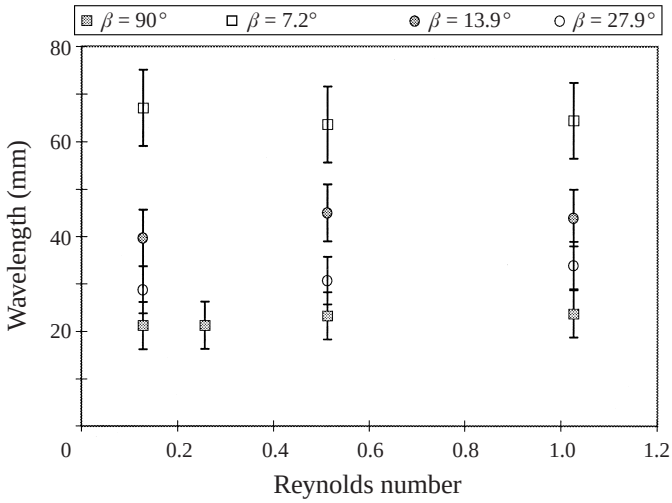

FIGURE 14. Wavelength as a function of Reynolds number and plate angle for Fluid B.

be partially due to the variation associated with the measured values for dynamic contact angles, which was typically 4°. The rounded shape of the rivulet tip makes measurement of the contact angle much more difficult than for a flat two-dimensional front where the shape of the front in the crossflow direction is much more uniform. Increasing the resolution of the images at the fluid front could greatly reduce the error of the data and help refine the relationship between the speed and contact angle of a fluid front. Note that U was limited by the capacity of the experimental setup to a small range of values and would have to be increased to validate a more complicated functional dependence.

4.2. *Unstable wavelength*

In figure 14 we plot the observed wavelength of the instability as a function of Reynolds number for $\beta = 7.2°$, 13.9°, 27.9° and 90° for Fluid B. As the angle of inclination of the plate is increased, the wavelength of the rivulet spacing decreases. In addition, we see almost no variation of wavelength with Reynolds number. The dependence of the wavelength on the other physical parameters can also be studied. One problem associated with the formation of rivulets is the tendency of neighbouring rivulets to merge into each other in an apparently random fashion, owing to small irregularities in the flow field. This is especially true at $\beta < 8.0°$, where the largest average difference in the experimentally measured wavelength occurred. The increased uniformity of the fluid front formed using the squeegee method helped to remedy this problem, along with repeated experiments to increase the experimental precision. This improved precision is evident by the error bars in figure 14, which represent the average deviation of the data calculated using the equation:

$$\text{Average deviation} = \frac{1}{n}|x - \overline{x}|, \tag{3}$$

where n is the number of data points ($n = 28$ for each average value for the wavenumber), x is the wavenumber for a single data point and $\overline{x}$ is the average wavenumber. The improvement is shown by the error being approximately 0.03 for the values of the wavenumber compared to a standard deviation of 0.06 for the wavenumber data of de Bruyn (1992).

Figure 14 shows that the wavelengths, within experimental error, were constant for varying values of *Re* for $\beta = 7.2^\circ$ to 90.0°. Each datum point represents the average wavelength value for approximately 30 experimental trials. The data followed the trend, predicted by the linear stability analysis of Lopez *et al.* (1996) for a constant-flux flow, that the wavelength λ increases with a decrease in β. The average wavelength values for $\beta = 7.2^\circ$, 13.9°, 27.9° and 90.0°, respectively, were 65.0, 42.9, 31.1 and 22.3 mm, corresponding to dimensionless wavenumbers (based on the measured upstream film thickness) of 40.6, 32.6, 29.4 and 28.2. On the other hand, de Bruyn (1992) found a dimensionless wavenumber, based on a computed average film thickness for the known volume per unit width, of 0.675 ± 0.060 for angles of inclination of 3° to 22° for a fixed volume of silicone oil on Plexiglas. Although the difference in the fluid used and material for the plate could possibly account for the different quantitative values for the wavelength of the instability of the flow, we still observe a similar trend for the effect that the angle of inclination of the plate has on the wavelength. De Bruyn calculated his values for the capillary length at a point where the fluid depth H_N reached 3 mm, which compares with a range for d_{0m} of 0.8 to 2.34 mm, as shown in table 2. The experimental results also differ from those of de Bruyn who found a constant wavenumber for silicone oil on Plexiglas over a similar range for β. However, the scaling parameter used was a capillary length, based on a constant volume of fluid, which ranged from 11.5 to 3.5 mm for $\beta = 2^\circ$ to 21°. Finally, we should note that in Lopez *et al.* (1997) these data were compared against a theory which included inertial terms. It appeared there that inertial theory compared better to the experimental results than a lubrication theory without inertial terms. What was not made clear is the fact that both theories which were compared to the experimental results also included a term which accounted for the effect of gravity normal to the interface. If neglected, both theories would have compared better with the results, and it would have been found that the Reynolds number would have little effect on the observed wavelength of the instability, as observed here.

Wavelength data were also taken for two other fluid mixtures besides Fluid A and B, with different viscosity and surface tension. The weight percentage of glycerin were 77% and 48% for the mixtures in the figures labelled Fluids C and D, respectively. Experimental results for the most unstable wavelength, λ_{max} as function of $d_{0m}/(3Ca)^{1/3}$ are given in figure 15 for the four fluids. The length $d_{0m}/(3Ca)^{1/3}$ was chosen because a scaling argument of Huppert (1982) implied that

$$\lambda_{max} = K d_{0m}/(3Ca)^{1/3} \tag{4}$$

where K is a constant. A least-square fit of the entire data set gives $K = 13.9$. The capillary number is calculated with the characteristic velocity determined by the volumetric flow rate, Q and the plate width. The result using equation (4) compares favourably with the values of K found experimentally to be approximately 18 by Huppert (1982) and 17 by Silvi & Dussan V. (1985), and numerically to be 14 by Troian *et al.* (1989). We see in figure 15 that the line formed by equation (4) fits almost all the data within the error of the experimental values for λ_{max}. However, if the power of the capillary term is not fixed, a better fit to the experimental data is given by

$$\lambda_{max} = 9.2 d_{0m}/(3Ca)^{0.45}, \tag{5}$$

which suggests a dependence of λ_{max} on $Ca^{-1/2}$, instead of $Ca^{-1/3}$ as given by Huppert. The experiments of Huppert (1982) and Silvi & Dussan (1985) used a constant volume of fluid, which resulted in time-varying, and much smaller, values of *Re*.

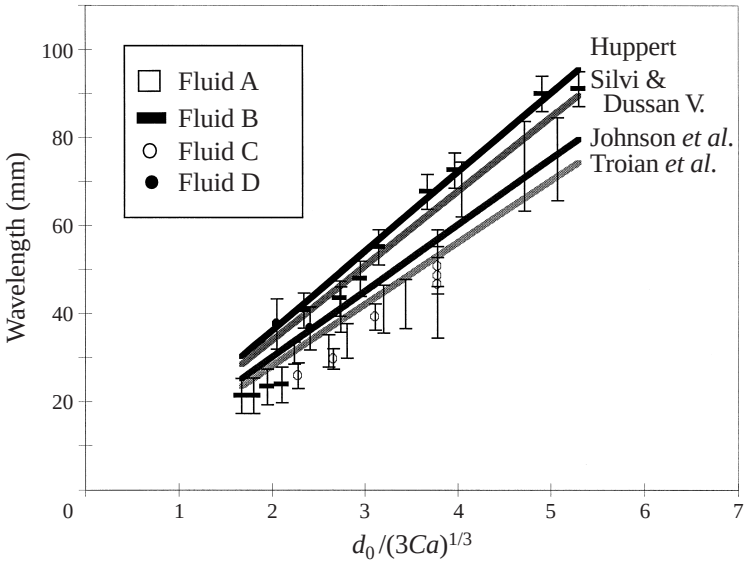

FIGURE 15. Comparison of experimental wavelength data (symbols) with the predictions of several models (lines).

5. Conclusions

An improved method for visualizing the entire flow field of a liquid sheet breaking up into rivulets on an inclined plate has been employed. Data for the wavelength for the instability of a two-dimensional front have been obtained for a fluid front supplied at constant volumetric flow rate, in contrast to other data for a fluid front formed from a constant volume of fluid. For the current range of plate inclination angles ($\beta = 7.2°$–$90.0°$) the rivulet wavenumber could be described by equation (4) as a function of the capillary number and fluid depth, d_{0m}, in agreement with the form of the equation proposed by Huppert (1982). However, there were significant differences, leading to questions about the appropriateness of comparing a constant-volume condition with that at constant-volumetric flux, as in the experimental flow conditions presented here.

Unique data were also obtained for the fluid depth profiles of the rivulets, giving insight into the varying, three-dimensional structure of the rivulets. The shape of the rivulets exhibited a dependence on the angle of inclination of the plate and the capillary number of the flow. Data were taken for a range of Reynolds and capillary numbers.

This work was supported by Basic Energy Sciences, Department of Energy through grant number FG02-86 ER 1364, National Science Foundation through grant number CTS 9223464 and by NASA Graduate Student Researcher Program, grant number NGT 51349.

REFERENCES

BERTOZZI, A. L. & BRENNER, M. P. 1997 Linear stability and transient growth in driven contact lines. *Phys. Fluids* **9**, 530–539.

BLAKE, T. D. 1993 *Dynamic Contact Angles and Wetting Kinetics.* Surfactant Science Series, vol. 49, pp. 251–309. Marcel Dekker.

Bruyn, J. R. de 1992 Growth of fingers at a driven three-phase contact line. *Phys. Rev.* A **46**, R4500–R4503.

Cazabat, A. M., Heslot, F., Troian, S. M. & Carles, P. 1990 Fingering instability of thin spreading films driven by temperature gradients. *Nature* **346**, 824–826.

Fraysse, N. & Homsy, G. M. 1993 An experimental study of rivulet instabilities in centrifugal spin coating of viscous Newtonian and non-Newtonian fluids. *Phys. Fluids* A **6**, 1491–1504.

Goodwin, R. 1991 An investigation of a viscous coating flow. PhD thesis, Stanford University, Stanford, CA.

Goodwin, R. & Homsy, S. H. 1991 Viscous flow down a slope in the vicinity of a contact line. *Phys. Fluid* A **3**, 515–528.

Hocking, L. M. 1990 Spreading and instability of a viscous fluid sheet. *J. Fluid Mech.* **211**, 373–392.

Hocking, L. M. & Miksis, M. J. 1993 Stability of a ridge of fluid. *J. Fluid Mech.* **247**, 157–177.

Huppert, H. E. 1982 Flow and instability of a viscous current down a slope. *Nature* **300**, 427–429.

Johnson, M. F. G. 1997 Experimental study of a thin liquid film flowing down an inclined plane. PhD thesis, Northwestern University.

Johnson, M. F. G., Schluter, R. A. & bankoff, S. G. 1997 Fluorescent imaging system for free surface flow. *Rev. Sci. Instrum.* **68**, 4097–4102.

Liu, J. L., Paul, J. D. & Gollub, J. P. 1993 Measurements of the primary instabilities of film flows. *J. Fluid Mech.* **250**, 69–75.

Lopez, P. G., Bankoff, S. G. & Miksis, M. J. 1996 Non-isothermal spreading on an inclined plane. *J. Fluid Mech.* **324**, 261–286.

Lopez, P. G., Miksis, M. J. & Bankoff, S. G. 1997 Inertial effects on contact line instability in the coating of a dry inclined plate. *Phys. Fluids* **9**, 2177–2183.

Melo, F., Joanny, J. F. & Fauve, S. 1989 Fingering instability of spinning drops. *Phys. Rev. Lett.* **63**, 1958–1961.

Moyle, D. T., Chen, M. S. & Homsy, G. M. 1999 Nonlinear rivulet dynamics during unstable dynamic wetting flows. *J. Multiphase Flow* (to appear).

Silvi, N. & Dussan V., E. B. 1985 On the rewetting of an inclined solid surface by a liquid. *Phys. Fluids* **28**, 5–7.

Spaid, M. A. & Homsy, G. M. 1996 Stability of Newtonian and viscoelastic dynamic contact lines. *Phys. Fluids* **8**, 460–478.

Troian, S. M., Herbolzheimer, S. A., Safran, S. A. & Joanny, J. F. 1989 Fingering instabilities of driven spreading films. *Europhys. Lett.* **10**, 25–30.